\$ STORY OF THE STO

Contents lists available at ScienceDirect

Earth and Planetary Science Letters

www.elsevier.com/locate/epsl



Assessing the presence of volatile-bearing mineral phases in the cratonic mantle as a possible cause of mid-lithospheric discontinuities



Sriparna Saha^{a,1}, Ye Peng^b, Rajdeep Dasgupta^{a,*}, Mainak Mookherjee^b, Karen M. Fischer^c

- ^a Department of Earth, Environmental and Planetary Sciences, Rice University, 6100 Main Street, MS 126, Houston, TX 77005, USA
- ^b Department of Earth, Ocean and Atmospheric Science, Florida State University, Tallahassee, FL 32306, USA
- ^c Department of Earth, Environmental and Planetary Sciences, Brown University, 324 Brook Street, Providence, RI 02912, USA

ARTICLE INFO

Article history: Received 21 June 2020 Received in revised form 22 September 2020

Accepted 23 September 2020 Available online 7 October 2020 Editor: A. Yin

Keywords: mid-lithospheric discontinuities cratons elastic moduli

elastic moduli pargasite phlogopite shear wave velocity

ABSTRACT

A number of possible hypotheses have been proposed to explain the origin of mid-lithospheric discontinuities (MLDs), typically characterized by \sim 2-6% reductions in seismic shear wave velocity (V_S) at depths of 60 km to \sim 150 km in the cratonic sub-continental lithospheric mantle (SCLM). One such hypothesis is the presence of low-shear wave velocity, hydrous and carbonate mineral phases. Although, the presence of hydrous silicates and carbonates can cause a reduction in the shear wave velocity of mantle domains, the contribution of volatile metasomatism to the origins of MLDs has remained incompletely evaluated. To assess the metasomatic origin of MLDs, we compiled experimental phase assemblages, phase proportions, and phase compositions from the literature in peridotite + H_2O , peridotite + CO_2 , and peridotite + H_2O + CO_2 systems at P-T conditions where hydrous silicate and/or carbonate minerals are stable. By comparing the experimental assemblages with the compiled bulk peridotite compositions for cratons, we bracket plausible proportions and compositions of hydrous silicate and carbonate mineral phases that can be expected in cratonic SCLMs. Based on the CaO and K2O contents of cratonic peridotite xenoliths and the estimated upper limit of CO_2 content in SCLM, $<\sim 10$ vol.% pargasitic amphibole, $\leq \sim 2.1$ vol.% phlogopite and $\leq \sim 0.2$ vol.% magnesite solid solution can be stable in the SCLM. We also present new elasticity data for the pargasite end member of amphibole based on first principles simulations for more accurate estimates of aggregate V_S for metasomatized domains in cratonic mantle. Using the bracketed phase compositions, phase proportions, and updated values of elastic constants for relevant mineral end members, we further calculate aggregate V_S at MLD depths for three seismic stations in the northern continental U.S. Depending on the choice of background wave speeds of unmetasomatized peridotite and the cratonic geotherm, the composition and abundance of volatile-bearing mineral phases bracketed here can explain as much as 2.01 to 3.01% reduction in V_S. While various craton formation scenarios allow formation of the amphibole and phlogopite abundances bracketed here, presence of volatile-bearing phases in an average cratonic SCLM composition cannot explain the entire range of velocity reductions observed at MLDs. Other possible velocity reduction mechanisms thus must be considered to explain the full estimated range of shear wave speed reduction at MLD depths globally.

© 2020 Elsevier B.V. All rights reserved.

1. Introduction

Cratons are the ancient cores of continents that have remained undisturbed by tectonic processes for as long as 2-3 billion years. The long-term stability of cratons has partly been attributed to the melt depleted nature of its underlying lithospheric mantle and

partly to its cold thermal structure (e.g. Boyd, 1989; Jordan, 1978). The cratonic sub-continental lithospheric mantle (SCLM) is characterized by depletions in incompatible elements such as Ca, K and Al and very high Mg#s \sim 92-94 (e.g. Boyd, 1989). Furthermore, variations in chemical depletion in cratonic xenolith samples suggest that these may have been modified by different processes and/or at different times (e.g. Griffin et al., 1988). Due to the low temperatures and distinct compositions of the SCLM, cratons are characterized by high aggregate shear wave velocities V_S , typically down to depths of 200-250 km (e.g. Gung et al., 2003; Lee et al., 2011; Steinberger and Becker, 2018). However, seismological in-

^{*} Corresponding author.

E-mail address: Rajdeep.Dasgupta@rice.edu (R. Dasgupta).

¹ Current address: School of Teacher Education and School of Earth and Environment, University of Canterbury, Private Bag 4800, Christchurch 8140, New Zealand.

vestigations have indicated the presence of a shear wave velocity reduction in the shallow cratonic SCLM (e.g. Thybo, 2006; Shearer and Buehler, 2019), and numerous studies around the globe have found decreases in V_S , typically by 2-6% at depths of 60 km to 150-160 km, features often called mid-lithospheric discontinuities (MLDs) (e.g. Rychert and Shearer, 2009; Abt et al., 2010; Fischer et al., 2010; Wolbern et al., 2012; Cooper and Miller, 2014; Hansen et al., 2015; Karato et al., 2015; Rader et al., 2015; Selway et al., 2015; Ford et al., 2016; Hopper and Fischer, 2018; Eilon et al., 2018; Kind and Yuan, 2018).

Given the widespread occurrence of MLDs in all cratons, numerous studies have considered varied models to explain their origins, including: (1) compositional layering due to a decrease in bulk Mg# with depth (e.g. Karato et al., 2015; Selway et al., 2015), (2) elastically accommodated grain boundary sliding, EAGBS (e.g. Karato et al., 2015), (3) layering in seismic anisotropy (e.g. Yuan and Romanowicz, 2010; Wirth and Long, 2014), (4) the presence of partial melt (e.g. Thybo, 2006), and (5) the presence of hydrous/carbonate mineral phases produced through metasomatism (e.g. Rader et al., 2015; Selway et al., 2015; Saha et al., 2018). While each of these proposed mechanisms has its own appeal, none of them are devoid of critique (e.g. Karato and Park, 2018). For example, reductions in V_S associated with gradual depletion are too small (<2%) to explain many MLD observations (e.g. Karato et al., 2015; Selway et al., 2015). Similarly, cratonic geotherms are typically too cold to permit the presence of partial melt (e.g. Karato et al., 2015). Although EAGBS can explain a single velocity reduction at MLD depths globally at modest temperatures (Karato and Park, 2018), its predictions are difficult to reconcile with some of the observed complexity in MLDs, including variations in MLD amplitude, continuity and depth (e.g. Hopper and Fischer, 2018). While some MLD observations also coincide with vertical changes in azimuthal anisotropy, (e.g. Yuan and Romanowicz, 2010; Wolbern et al., 2012; Wirth and Long, 2014) this is not true in general (Ford et al., 2016).

The presence of hydrous or carbonate accessory minerals such as amphibole, phlogopite, or chlorite can cause velocity reductions at MLDs (e.g. Eeken et al., 2018; Rader et al., 2015; Selway et al., 2015). In fact, samples from a potentially representative MLD-related layer (Wang and Kusky, 2019) are found to be rich in minerals like amphibole, phlogopite, chlorite, and carbonates that form as a consequence of metasomatism. While the dynamic stability of volatile-bearing partial melts is questionable, volatile-bearing hydrous/carbonate mineral phases formed by interaction of such melts or fluids with the cratonic mantle can lead to reduction in aggregate V_S (e.g. Rader et al., 2015; Selway et al., 2015; Saha and Dasgupta, 2019). Several existing studies (e.g., Rader et al., 2015; Hopper and Fischer, 2015) posit the presence of more than 10% phlogopite in volatile-rich layer(s) as a plausible explanation for MLDs.

However, it remains unclear whether such compositional layering can be expected globally. One issue with metasomatic origins for MLDs is their ambiguous relationship to conductivity anomalies (e.g. Selway, 2019; Karato and Park, 2018). Mantle metasomatism as the cause of MLDs has also been critiqued on grounds that it would reset the age of lithospheric rocks, and evidence for such age stratification is lacking (Karato and Park, 2018). Age data that favors metasomatic MLD origins is provided by Hopp et al. (2008), a study that used 40 Ar/ 39 Ar to determine a 1-1.25 Ga age for phlogopite from Kaapvaal craton kimberlites, tying the phlogopite to later orogenic metasomatism of the Archean Kaapvaal mantle. However, such observations are sparse, and metasomatism that significantly postdates cratonic formation may not be the explanation of MLDs in all continents. On the other hand, volatile metasomatism may have occurred during craton formation, and further investigation is needed regarding how the fractions and

compositions of volatile-bearing phases stabilized in the ambient cratonic mantle influence the seismic properties of the SCLM.

Currently, it is unclear how the presence, modes, and compositions of volatile-bearing phases vary as a function of craton refertilization history and bulk composition. Hydrous minerals like amphibole, mica, chlorite, and carbonate minerals have diverse chemistry, but the bulk compositional range and P-T conditions of cratonic SCLM must control the abundance and composition of mineral end members in natural systems. For example, low abundances of major oxides such as CaO and K2O in the cratonic SCLM (Figs. 1c and 1f), along with H2O, can limit proportions of volatile-bearing mineral phases, such as amphibole and/or phlogopite, respectively (e.g. Saha and Dasgupta, 2019). However, local metasomatic processes can lead to higher abundance of CaO and K₂O as evident by the spread in the oxide data in Figs. 1a and 1b, potentially allowing formation of high proportions of these volatile-bearing mineral phases. High proportions of hydrous minerals may lead to rheological weakening of the craton, resulting in convective removal thus challenging the long-term stability of cratons (Lee et al., 2011). Yet, according to analyses of natural data by Tommasi et al. (2017), presence of amphibole and phlogopite does not cause significant weakening of the mantle. Nonetheless. its potential dynamic implications highlight the need for evaluating the metasomatic model for the MLD by constraining the proportions and compositions of the volatile-bearing phases that may exist in the cratonic SCLM.

The mineral end member composition prevalent in the SCLM is controlled by its bulk compositional range. End member compositions of minerals may have different thermoelastic properties that can affect aggregate V_S. In particular, for estimation of aggregate V_S shear moduli of mineral phases remain poorly constrained in the literature; most existing databases for elastic properties of mineral end-members (e.g. Abers and Hacker, 2016) do not account for variation in the physical properties arising due to compositional variability. For example, bulk moduli (K) for the different end members of amphibole in the database of Abers and Hacker (2016) are based on an earlier thermodynamic database by Holland and Powell (1998) and equation of state results (Comodi et al., 1991). Abers and Hacker (2016) also estimate the shear moduli (G) for amphibole using constant Poisson's ratio without considering any compositional dependence which can result in inaccurate estimates of V_S. Additionally, the pressure and temperature dependencies of elasticity for volatile bearing phases are poorly constrained. Thus, to evaluate the role of hydrous minerals such as amphibole and phlogopite in affecting the aggregate V_S there is a need to consider not only appropriate compositions and proportions of mineral phases, but also thermoelasticity of the relevant end-members dominant in the natural system (Brown and Abram-

The main aim of this study is thus to evaluate the control of compositional parameters (e.g. CaO, K2O, H2O and/or CO2) of peridotites on the stability, chemistry, and abundances of volatile bearing phases to evaluate aggregate shear wave velocity reductions at MLD depths in cratons. More than four decades of laboratory experiments have investigated the effects of major volatile oxides, i.e., H₂O and/or CO₂, on the high pressure phase relations of mantle peridotites exhibiting varying degrees of fertility over a wide range of pressure and temperature (P-T) conditions. The stability and composition of the volatile-bearing minerals in these systems has been evaluated critically (e.g. Lara and Dasgupta, 2020; Mallik et al., 2015; Mandler and Grove, 2016; Mengel and Green, 1989; Tumiati et al., 2013). However, a systematic evaluation of how bulk composition controls the mineral chemistry and abundance of the volatile bearing phases is lacking and is key in assessing the role of volatile-bearing phases in influencing the seismic properties of cratons.

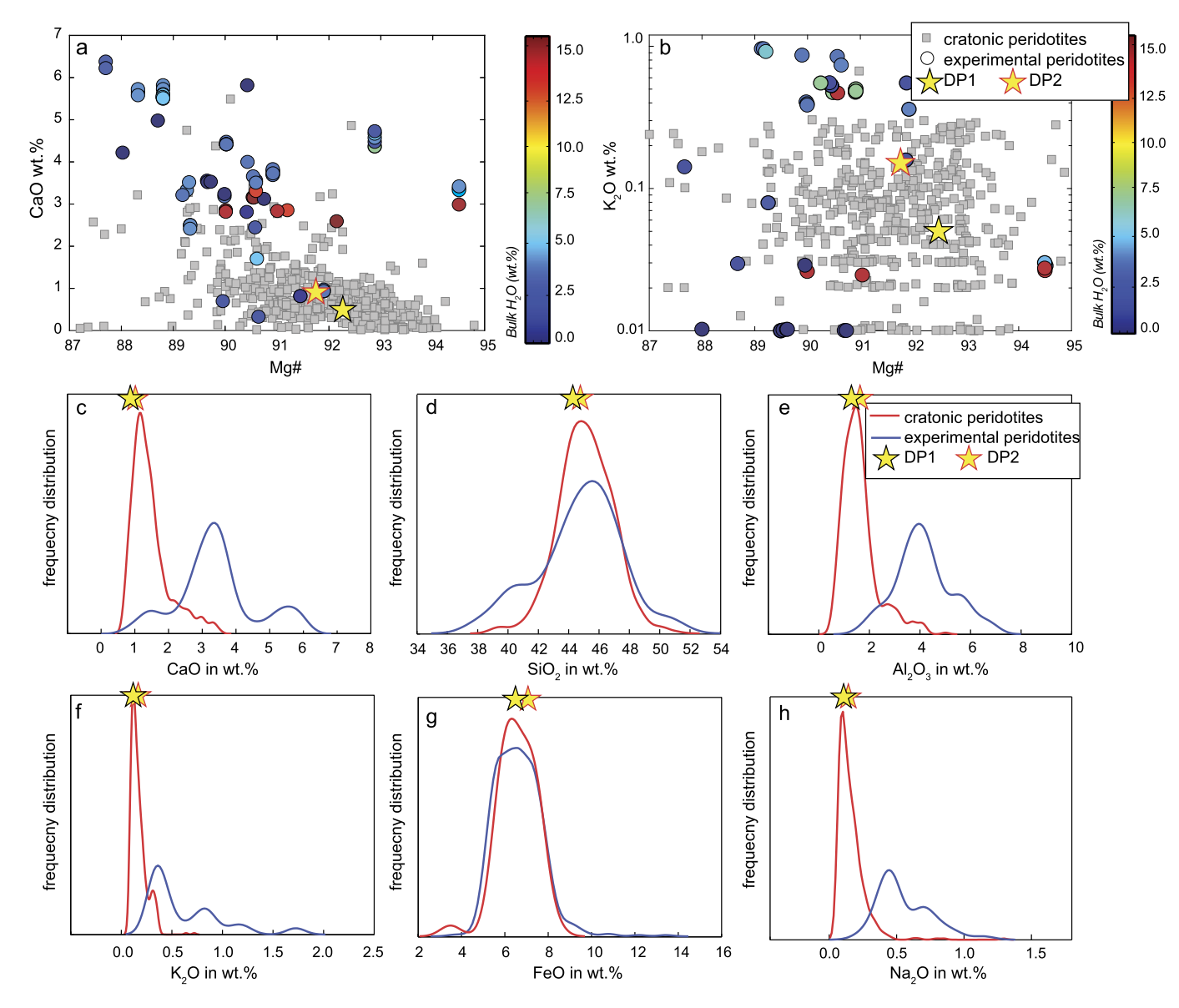


Fig. 1. (a) CaO and (b) K_2O contents reported in cratonic xenolith samples filtered for contamination plotted as a function of bulk Mg# (Table S3; Lee et al., 2011; Luguet et al., 2015). Variation in CaO and K_2O contents in experimental peridotite $\pm H_2O \pm CO_2$ bearing systems (Table S1) are also plotted for reference and are depicted by the colored circles where the color bar corresponds to the bulk H_2O . (c-h) Frequency distributions for different major element oxides in the natural and experimental peridotite systems shown in (a) and (b) are plotted in red and blue, respectively. Based on the major element oxide distributions reported in the cratonic peridotite xenoliths, two bulk compositions representative of the SCLM (solid stars) DP1 and DP2 are identified and used for estimating variation in background aggregate shear wave velocities V_{SB} for the SCLM. (For interpretation of the colors in the figure(s), the reader is referred to the web version of this article.)

Here, we compile experimental phase assemblages, phase proportions, and phase compositions from the literature in peridotite + H₂O, peridotite + CO₂, and peridotite + H₂O + CO₂ systems at P-T conditions where hydrous silicate and/or carbonate minerals are stable. By comparing bulk compositions for experimental assemblages with compiled bulk peridotite compositions for cratons, we bracket plausible proportions and compositions of hydrous silicate/carbonate mineral phases that can be stable in cratonic SCLMs. We also present and incorporate new elasticity data for the pargasite end member of amphibole based on first principles simulations. Using the bracketed compositions and proportions of phases and updated values of elastic parameters for mineral end members of relevance, we calculate aggregate V_S at cratonic SCLM depths for average compositions expected globally. Plausible estimates of aggregate V_S in cratonic SCLMs and their comparison with seismic data yield the extent to which MLDs can be explained by the presence of volatile-bearing mineral phases. Finally, a comparison between observed (natural) and estimated seismic shear velocities helps to assess plausible metasomatic processes that might have produced MLDs.

2. Methods

To assess the stability, composition, and abundances of hydrous/carbonate phases at MLD depths in cratonic SCLMs, we compiled 237 previously published peridotite phase equilibria experiments in $\rm H_2O \pm \rm CO_2$ bearing systems (Tables S1 and S2). Because this study aims to evaluate the presence of hydrous/carbonate silicate phases as potential causes for velocity reductions at MLD depths, super-solidus experiments where hydrous/carbonate mineral phases are absent were excluded. Similarly, serpentinite bulk compositions effectively devoid of Ca and K, essential for the formation of minerals like amphibole and/or phlogopite, were excluded as well (e.g. Sieber et al., 2018). The compilation includes peridotite phase relation experiments conducted over a wide range

Table 1Modified thermoelastic database from Abers and Hacker (2016) used in this study to generate velocity profile of MLD region.

End members	Bulk modulus K _T (GPa)	dK _T /dP	Shear modulus G (GPa)	dlnG/dln $ ho$	dG/dP	First Gruneisen parameter Yth	Second Gruneisen parameter δ_{T}
Forsterite	127.3 ^{b*}	4.20 ^{c*}	81.6 ^{b*}	5.19 ^{a*}	1.6 ^{c*}	1.29 ^{e*}	5.5 ^{e*}
(olivine)	120.20*	4.000*	54.000*	4.000*	4 = 4 d*	1.040*	F 40*
Fayalite (olivine)	136.3 ^{c*}	4.88 ^{c*}	51.22 ^{c*}	4.69 ^{a*}	1.71 ^{d*}	1.21 ^{e*}	5.4 ^{e*}
Enstatite	107.9 ^{f*}	6.6^{h^*}	77.9 ^{f*}	7.55 ^{a*}	1.9^{i^*}	0.95^{a^*}	7.55^{a^*}
(orthopyroxene)							
Ferrosilite	100.1 ^{g*}	6.6^{a^*}	52 ^{g*}	7.74^{a^*}	1.9^{a^*}	1.14^{a^*}	7.74^{a^*}
(orthopyroxene)	i*	. =1*	o i*	. ;*		i*	. = i*
Diopside	116.5 ^{j*}	4.5^{l^*}	72.8 ^{j*}	4^{j^*}	1.9 ^{a*}	1.1 ^{j*}	4.5^{j^*}
(clinopyroxene)	120.5 ^{k*}	4.5^{a^*}	61.8 ^{k*}	6^{a^*}	1.9^{a^*}	1.5 ^{m*}	6^{a^*}
Hedenbergite (clinopyroxene)	120.5"	4.5"	61.8"	6"	1.9"	1.5***	6"
Pyrope	167.3 ^{n*}	4.1^{n^*}	94^{n^*}	4.06^{a^*}	1.3 ^{n*}	1.25 ^{e*}	5.3 ^{e*}
(garnet)							
Grossular	163.9^{n^*}	3.9^{n^*}	109^{n^*}	5.11^{a^*}	1.1^{n^*}	1.19^{e^*}	4.57^{e^*}
(garnet)							
Almandine	170.3^{n^*}	4.9^{n^*}	96^{n^*}	5.52^{a^*}	1.4 ^{n*}	1.07^{a^*}	5.52^{o^*}
(garnet)	-*	-*	-*	-*	_*	-*	*
Magnesite	97.1 ^{p*}	5.44 ^{p*}	58 ^{a*}	3.3 ^{a*}	1.0^{a^*}	1.58 ^{a*}	3.3^{p^*}
(carbonate)	0 = 00	0	00 =0	0.07		0.09(1)	0.07
Pargasite	95.3 ^q	5.4 ^q	60.7 ^q	9.8 ^q	1.2 ^q	$0.9^{q(1)}$	8.2 ^q
(amphibole) Edenite	91.8 ^r	$5.4^{q(2)}$	56.3 ^r	10.5 ^{q(2)}	1.2 ^{q(2)}	$0.9^{q(1)}$	$8.5^{q(2)}$
(amphibole)	31.0	5.4	30.5	10.5	1,2	0.5	0.5
Katophorite	88.5 ^r	$5.4^{q(2)}$	54.1 ^r	$11.0^{q(2)}$	$1.2^{q(2)}$	$0.8^{q(1)}$	$8.9^{q(2)}$
(amphibole)	55.5		- ***	- 110		0	5.0
Richterite	86.6 ^r	$5.4^{q(2)}$	56.8 ^r	$10.5^{q(2)}$	$1.2^{q(2)}$	$0.8^{q(1)}$	$9.1^{q(2)}$
(amphibole)							
Phlogopite	52.0 ^s	6.5 ^s	33.7 ^s	$16.1^{q(6)}$	2.1 ^s	$0.6^{q(3)}$	$16.1^{u(4)}$
(mica)							
Clinochlore	79.2 ^t	3.7^{t}	47.4 ^t	$15.3^{q(6)}$	-0.3^{t}	$0.5^{q(5)}$	15.3 ^{u(4)}
(chlorite)							

^{*} indicates parameters that are listed from the database of Abers and Hacker (2016). $^{\rm q}$ refers to the data generated in this study. The lettered superscripts a-u refer to the original references and the numbered superscripts 1-6 are notes on thermodynamic parameters and both are explained in details in the Supplementary Material. $K_{\rm T}$ represents isothermal bulk modulus and G represents shear modulus measured at standard temperature and pressure (STP). $dK_{\rm T}/dP$ and dG/dP are pressure derivatives of G and G respectively. G and G represent the first and second G respectively.

of P (0.5-8 GPa), T (680-1300 °C), and bulk compositions (CaO: \sim 0.28-6.38 wt.%, K_2O : \sim 0.00-6.38 wt.%, H_2O : 0.05-15.97 wt.%, CO_2 : 0.50-8.00 wt.%) where minerals like amphibole, phlogopite, carbonates or chlorite are stable. Available information from each experiment includes P, T, equilibrium mineral assemblage, phase compositions, and phase proportions. Mineral abundances were estimated using mass balance calculations for some experimental studies that did not report them, subject to availability of phase compositional data (see footnotes in Table S1). The available and calculated mineral abundances were used to recalculate mineral mass fractions (on a melt-free basis) based on available mineral compositions.

To examine the full range and the dominant composition of cratonic SCLM in terms of major and minor element chemistry, and compare experimental bulk compositions with natural mantle compositions, cratonic xenolith bulk compositional data were also compiled (Table S3; e.g., Lee et al., 2011; Luguet et al., 2015) from previous studies and filtered for contamination (Fig. 1). Xenolith major element bulk compositions were used to identify the most relevant experimental bulk compositions for cratonic SCLMs at MLD depths. *P-T* estimates reported for these peridotite xenoliths range from 2 to 6 GPa and 600 to 1200 °C respectively, thus covering the depth range at which most MLD occurrences in cratons are reported.

Mineral mass fractions (Table S1) and reported mineral compositions from the experimental compilation (Table S2) recalculated on a melt free basis were used to calculate modal abundance

(vol.%) of the constituent mineral end members (reported in Table S4). This was done using the density of each end member at the *P-T* condition of interest following the approach of Abers and Hacker (2016).

In order to most accurately determine the seismic properties of the assemblage, we (1) updated the existing thermoelastic database (Abers and Hacker, 2016) using recent data on bulk (K) and shear moduli (G), and their pressure and temperature derivatives (Table 1) and (2) determined the thermoelastic parameters for end-member amphibole pargasite since this is one of the most important volatile-bearing phase end members that can be stable in metasomatized peridotite and little is known about its elastic properties. The high pressure elasticity of pargasite, (NaCa₂(Mg₄Al)(Si₆Al₂)O₂₂(OH)₂), was determined using first principles simulations based on density functional theory (DFT) (Hohenberg and Kohn, 1964) and the details are included in the Supplementary Materials. Updated elasticity data for pargasite (reported here), phlogopite (Chheda et al., 2014), chlorite (Mookherjee and Mainprice, 2014), and other relevant mineral end members (Supplementary Materials) were used to update the MS Excel macro of Abers and Hacker (2016) (Table 1). The estimated modal abundances and respective P-T conditions were then used as input for the updated MS Excel macro of Abers and Hacker (2016), to calculate the aggregate V_S. These estimates were compared with the aggregate V_S values reported in several cratons to evaluate if velocity reductions at MLDs can be caused

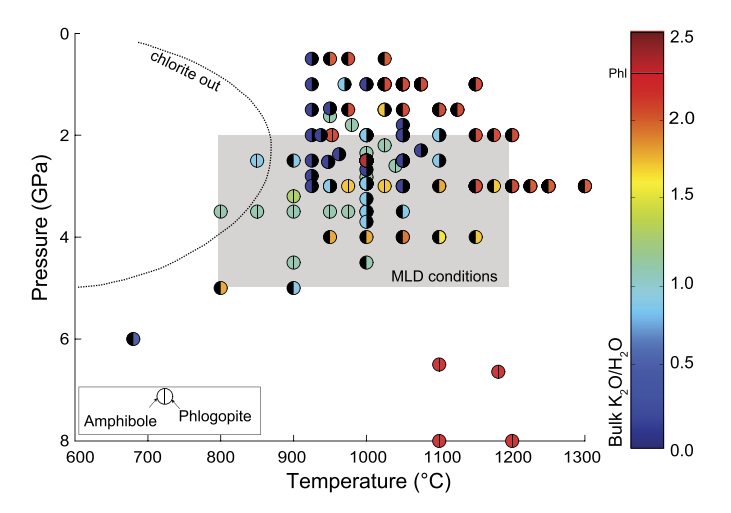


Fig. 2. *P-T* space depicting stability of amphibole and phlogopite for experimental peridotite + H₂O \pm CO₂ bearing systems (Table S1). The left and right halves of the circle represent amphibole and phlogopite respectively; the absence of a phase is marked in black. Colored portions correspond to bulk K₂O/H₂O denoted by the color bar, which also marks the K₂O/H₂O ratio of phlogopite (Phl) – cooler colors below the Phl mark suggest fluid-present experiments whereas warmer colors above the Phl mark indicate fluid-absent experiments. *P-T* conditions relevant for the MLD depth range are marked by the grey box. Chlorite-out boundary from Till et al. (2012) and Grove et al. (2006) is marked by the dashed black line. (For interpretation of the colors in the figure(s), the reader is referred to the web version of this article.)

by volatile-bearing crystalline phases expected for SCLM compositions.

3. Results

3.1. Stability of volatile-bearing phases at MLD depths: bulk compositional control

The compiled experiments (Table S1) reveal that in addition to the volatile-free silicate minerals, amphibole and/or mica \pm chlorite and/or mineral carbonates such as dolomite and/or magnesite can be stable in the cratonic SCLM. The hydrous phase stable in the peridotitic system depends on bulk composition and the P-T conditions. For example, chlorite is stable only in aqueous fluid-saturated conditions with bulk $H_2O>9$ wt.% and low $K_2O~(\sim\!0\text{-}0.026~\text{wt.\%})$, at temperatures $\leq\!840\,^{\circ}\text{C}$ between 2.8 and 3.2 GPa and $\sim\!680\,^{\circ}\text{C}$ at 4 GPa (Table S1). The upper limit of the stability field of chlorite (Fig. 2) thus indicates that chlorite is stable at conditions that correspond to the shallower and colder end of the P-T range expected at MLD depths.

Phlogopite and amphibole, on the other hand, are stable in systems with bulk $\rm H_2O$ as low as ~ 0.2 wt.%. Their stability is controlled by a combination of bulk alkali and $\rm H_2O$ contents in addition to their P-T stability field (Fig. 2). We note that in systems with high bulk $\rm K_2O/H_2O$ (Fig. 2), amphibole is not stable at $P \sim 1\text{-}4$ GPa. These experiments correspond to $T > 900\,^{\circ}\text{C}$ and the absence of amphibole at these conditions can be attributed to the temperature stability limit for pargasitic amphibole. In contrast, for a similar temperature range at $P \sim 6\text{-}8$ GPa, richteritic amphibole is stable even for high bulk $\rm K_2O/H_2O$, corresponding to high bulk $\rm K_2O$ in the systems. Phlogopite on the other hand, is absent in systems with low bulk $\rm K_2O/H_2O$ (Fig. 2). Low bulk $\rm K_2O/H_2O$ in these systems can be attributed to the low bulk $\rm K_2O$ in the systems, which potentially limits phlogopite formation.

However, amphibole and phlogopite co-exist for intermediate values of bulk $K_2O/H_2O\sim0.5$ -1.5 at *P-T* conditions relevant for the cratonic SCLM and hence are more likely candidates for velocity reductions at MLD depths. In addition to hydrous silicate minerals,

magnesite and/or dolomite solid solutions are stable in peridotite + CO $_2$ \pm H $_2$ O systems, with bulk CO $_2$ as low as 0.5 wt.% (e.g. Saha et al., 2018) between 1.6 and 6.6 GPa straddling the MLD depth range for cratons.

3.2. Bulk composition dependence of mineral chemistry

Chlorite stable in the hydrous peridotitic bulk compositions of Mg# \sim 90-91 is compositionally close to clinochlore, with Mg# \sim 85-92, and the experiments represent the shallower and the colder end of the *P-T* range expected at MLD depths.

Amphibole compositions in volatile bearing peridotite systems vary as a function of bulk (a) CaO and (b) alkali contents (Fig. S1). For example, in peridotitic systems with bulk CaO ≥ 0.5 wt.%, amphiboles are broadly calcic, but show variation in their chemistry depending on the bulk alkali content, i.e., when total alkali ≥ 0.5 wt.%, amphiboles are pargasite-edenitic and for total alkali <0.5 wt.%, amphiboles are Mg-hornblende-tschermakitic. In systems with bulk CaO < 0.5 wt.%, amphibole chemistry evolves towards the sodic-calcic end and classifies as either magnesio-katophorite or K-richteritic. Therefore, amphibole compositions in the cratonic SCLM relevant for the MLD depths range from pargasitic-edenitic to tschermakitic-katophoritic.

The mica composition that is stable in peridotitic bulk compositions is phlogopitic with an annite component <3.2 wt.%. Phlogopite compositions vary little with bulk K_2O contents ranging between 0.03 and 1.58 wt.% and bulk H_2O contents between 0.05 and 13.79 wt.%.

Carbonate stable in the CO_2 -bearing peridotitic systems is magnesite and/or dolomite solid solution depending on the P-T conditions and bulk composition. At $P \leq 3$ GPa, the stable carbonate phase is dolomite at $\sim 1000\,^{\circ}\text{C}$ co-existing with magnesite in fertile bulk compositions (e.g. Falloon and Green, 1989; Dasgupta and Hirschmann, 2006; Tumiati et al., 2013). However, systems depleted in CaO stabilize magnesite as the only carbonate phase even at pressures as low as 2 GPa (e.g. Saha et al., 2018; Saha and Dasgupta, 2019).

3.3. Abundance of volatile-bearing mineral phases in the SCLM: control of bulk compositions

3.3.1. Chlorite

Modal abundances for chlorite are constrained in four experimental studies on peridotitic compositions (Dvir et al., 2011; Fumagalli and Poli, 2005; Grove et al., 2006; Till et al., 2012). Bulk compositions explored in these studies differ mainly in their bulk $\rm H_2O$ contents. These experimental studies, relevant for subduction zone settings, suggest that $\sim\!16$ wt.% of chlorite can be present in mantle wedge conditions corresponding to $\sim\!2$ wt.% bulk $\rm H_2O$ in the mantle (e.g. Till et al., 2012). Considering the dehydrated nature of the cratonic SCLM (e.g. Peslier et al., 2010), the aforementioned chlorite abundance can be representative of extensively hydrated domains unlikely to occur in the cratonic SCLM.

3.3.2. Amphibole

Amphibole abundance in peridotite systems is controlled by a combination of bulk CaO, alkali, H_2O , and temperature (Fig. 3). We note that amphibole abundance increases with greater bulk CaO and is as high as \sim 35 wt.% when CaO contents are \geq 5 wt.%. However, as evident from the overlap between experimental and natural cratonic peridotite compositions in Fig. 1(c), in metasomatized pockets, CaO can reach 2-3 wt.% and thus \leq 10-15 wt.% of amphibole is more realistic for the cratonic SCLM. Amphibole abundance also increases with decreasing temperature and decreases with higher bulk alkali/ H_2O at a given CaO and temperature. For the dominantly observed CaO contents (<1 wt.%) in the cratonic SCLM

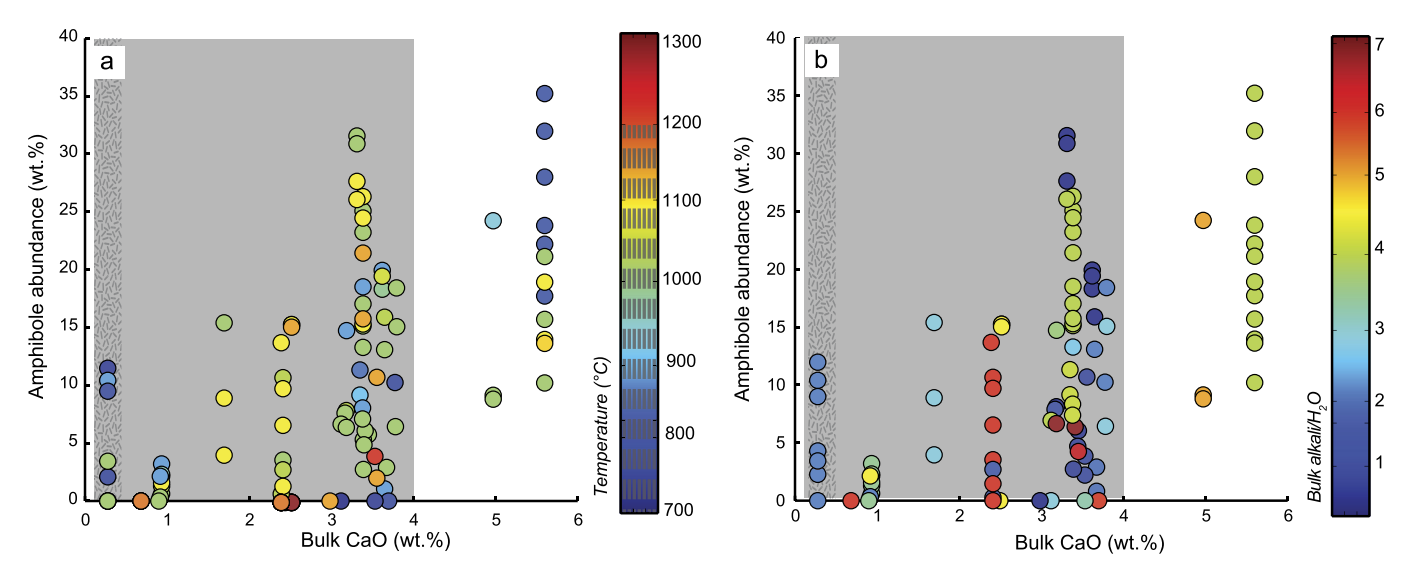


Fig. 3. Variation in amphibole abundance from various experimental studies (Table S1) with bulk CaO plotted as a function of (a) temperature and (b) bulk alkali/ H_2O . Stippled region in the color bar in panel (a) indicates the range of temperature found in cratons at MLD depths. The grey stippled, vertical bands in the plots correspond to the most frequent abundance of CaO found in cratonic peridotite xenoliths and the grey shaded, vertical bands represent the maximum range of overlap between experimental peridotite systems and natural peridotite samples from cratonic regions as observed from Fig. 1. (For interpretation of the colors in the figure(s), the reader is referred to the web version of this article.)

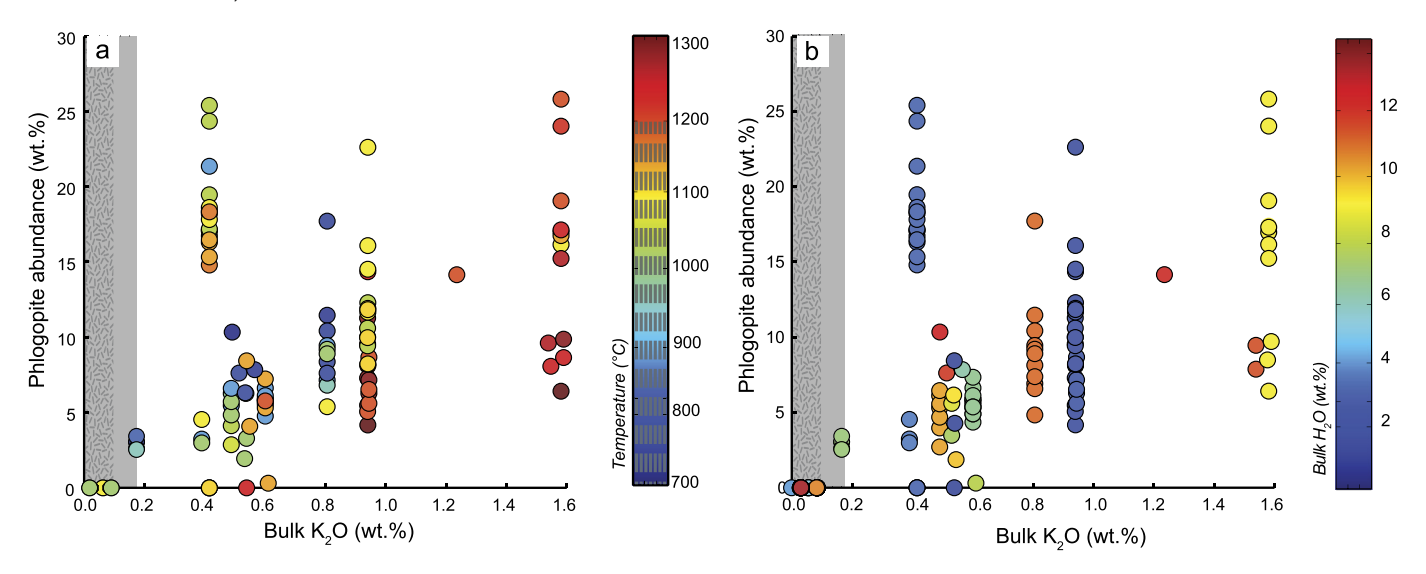


Fig. 4. Variation in phlogopite abundance from various experimental studies (Table S1) with bulk K_2O plotted as a function of (a) temperature and (b) bulk H_2O contents. Stippled region in the color bar represents the range of temperature found in cratons at MLD depths. Grey stippled portions in the plots correspond to the dominant abundance of K_2O found in cratonic peridotite xenoliths; the grey shaded band represents the maximum range of overlap between experimental peridotite systems and natural peridotite samples from cratonic regions as observed from Fig. 1. (For interpretation of the colors in the figure(s), the reader is referred to the web version of this article.)

(grey stippled band in Fig. 3), up to 10 wt.% (\sim 10 vol.%; 2000 ppm H₂O) of amphibole can be stable in the cratonic mantle at MLD depths.

3.3.3. Phlogopite

The compositional parameters that control phlogopite abundance are bulk K_2O and bulk H_2O contents (Fig. 4). We note that phlogopite abundance increases with increasing K_2O content and that presence of ~ 1.6 wt.% of bulk K_2O in the system can stabilize up to 25 wt.% phlogopite. However, excess H_2O availability can limit phlogopite abundance (Green et al., 2014; Saha and Dasgupta, 2019). Finally, for the most dominant composition sampled in the SCLM i.e., ~ 0.15 -0.17 wt.% K_2O (Fig. 1f), no more than 5 wt.% (~ 5 vol.%; 2000 ppm by weight H_2O) of phlogopite can be stable (Fig. 4). Considering K_2O mass balance alone, however, suggests that the maximum phlogopite (containing ~ 8 -10 wt.% K_2O)

abundance is \leq 1.5-2.1 wt.%, i.e., if phlogopite is the only K-bearing phase and no melt or fluid is stabilized.

3.3.4. Magnesite solid solution

Unlike hydrous phases, the abundance of which show some dependence on the major element compositions of peridotite, the phase proportions of magnesite vary only with bulk CO₂. Magnesite abundance increases with increasing bulk CO₂ content and decreases with increasing temperature, in particular across the solidus. However, the CO₂ content of the cratonic SCLM is poorly constrained because carbonated peridotite undergoes decarbonation during exhumation (e.g., Canil, 1990). With the average upper bound of \sim 750-1000 ppm CO₂, as argued based on a carbon cycle box model (Lee et al., 2019), \leq 0.2 wt.% magnesite can be expected at shallow MLD depths. Although we chose \sim 1000 ppm CO₂ as the upper bound, a greater abundance of magnesite lo-

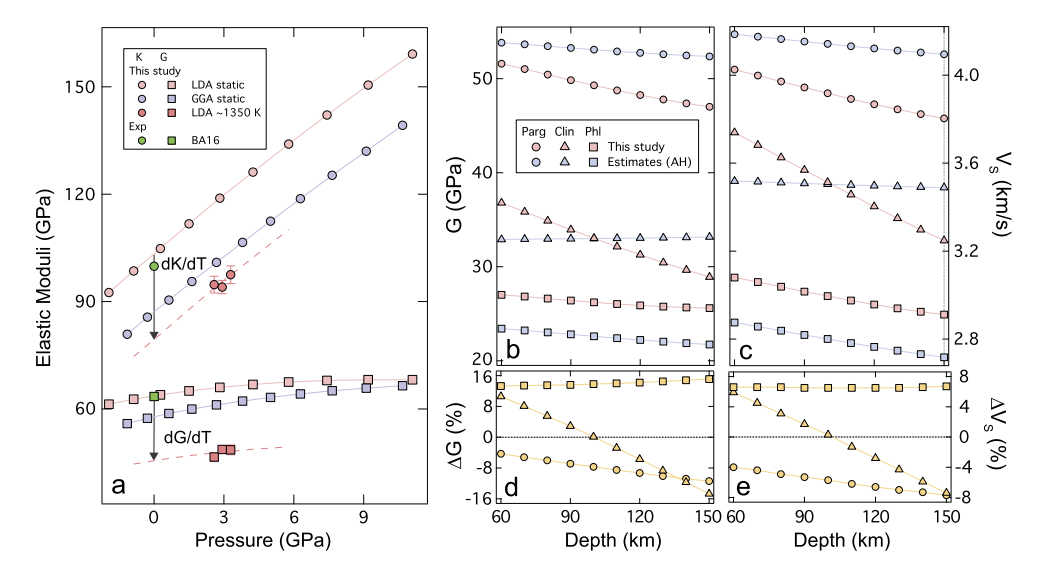


Fig. 5. (a) Bulk and shear moduli for pargasite amphibole as a function of pressure- pink and blue symbols refer to results from local density approximation (LDA) and generalized gradient approximation (GGA) respectively. Red symbols with error bars refer to results from FPMD (LDA) at ~1350 K (details of the method could be found in the supplementary section). Green symbols (BA16) refer to zero-pressure experimental results (Brown and Abramson, 2016). Temperature derivatives of bulk and shear modulus are shown depicted by black arrows. (b-c) Comparison of (b) shear modulus and (c) shear wave velocity predicted using *first principles* simulation (this study) and the earlier estimates (AH: Abers and Hacker, 2016) at depths corresponding to MLDs. The (b) shear modulus and (c) shear wave velocity is calculated along a geotherm with a surface heat flux of 45 mW/m² (Artemieva, 2009). (d-e) The percentage difference of (d) shear modulus and (e) shear wave velocity between this study and the previous estimates (AH: Abers and Hacker, 2016) at MLD depths, where $\Delta G = 100\% \times (G - G^{AH})/G^{AH}$ and $\Delta V_S = 100\% \times (V_S - V_S^{AH})/V_S^{AH}$. The black dashed lines indicates the line of zero deviation between *first principles* prediction (this study) and earlier estimates. Positive deviation from the zero line indicates that our prediction is softer or seismically slower than the previous estimates (Abers and Hacker, 2016) heigend: pargasite (parg) – circle; clinochlore (clin) – triangle; phlogopite (phl) – square.

cally, over a narrow depth range at or around MLDs, cannot be completely ruled out for domains that suffer more focused carbonatitic or other $\rm CO_2$ -rich melt influx (e.g., Foley and Fischer, 2017; Sun and Dasgupta, 2019, 2020). However, we argue that given the average upper limit of $\rm CO_2$ in the SCLM is \sim 750-1000 ppm, higher abundance of magnesite at MLD depths globally is unlikely.

3.4. Thermoelastic parameters

Our first principles simulations of the crystal structure, equation of state, and elasticity of pargasitic amphibole agree well with previous experimental studies (Figs. S2-S5). We find that pargasitic amphibole has G of 60.7 GPa (Table S7: Fig. 5) which is in excellent agreement with recent experimental results of 59.5-62.6 GPa (Brown and Abramson, 2016). The first principles simulation results of G for tremolite (Peng and Mookherjee, 2020) and glaucophane (Mookherjee and Bezacier, 2012) end member amphibole are also in very good agreement with experimental results with differences of \sim 0.7% and 2.2% (Brown and Abramson, 2016; Bezacier et al., 2010). However, most experimental results for G are limited to ambient conditions. Given the good agreement between the first principles simulations and the experimental results at ambient condition, we find the pressure derivative of G, dG/dP to be 1.16 and the temperature derivative of G, dG/dT to be -13.4 MPa/K (Fig. 5; Supplementary Material). So far, the available dG/dP data for amphiboles are only from first principles simulation, i.e., 1.3 for tremolite (Peng and Mookherjee, 2020) and 2.0 for glaucophane (Mookherjee and Bezacier, 2012). Recently, dG/dT for tremolite was reported; however, it was derived from dK/dT (Peng and Mookherjee, 2020). So this study presents the first result of dG/dT for amphiboles using first principles molecular dynamics (FMPD) (Supplementary Method). At depths corresponding to MLDs, i.e., 60 km to \sim 150 km, the shear modulus of pargasite is 4-11% softer than previous estimates (Abers and Hacker, 2016). The softer shear modulus translates to a seismically slower V_S of pargasite by 4-8% compared to previous estimates (Fig. 5) (Abers and Hacker, 2016).

4. Discussion

4.1. Aggregate shear wave velocities of SCLMs at MLD depths – control of volatile-bearing mineral phases

Here we calculate aggregate shear wave velocities based on our compiled experimental phase relations, taking into account the compositional intersection between experimental compositions and those of natural SCLM xenoliths, and the updated thermoelastic parameters of relevant mineral end members.

Estimates for the shear wave speed for the chlorite bearing experimental assemblages indicate that the presence of \sim 16 to 20 wt.% chlorite at 3.2 to 4.0 GPa can lower V_S by \sim 0.40-1.35% which is lower than the typical range of V_s reduction reported for MLDs and may be similar to MLD occurrences that record minimal velocity reductions. Additionally, the aforementioned abundance of chlorite corresponds to \sim 2 wt.% H₂O in the SCLM (Grove et al., 2006), which considering the dehydrated nature of the cratonic SCLM (e.g. Peslier et al., 2010) is not feasible. Furthermore, given chlorite is stable only at high water fugacity and at extremely depleted bulk compositions and at low pressures and cooler temperatures, we argue chlorite's role in causing velocity reductions at most MLD depths is minimal. Our claim is also supported by the rare occurrence of chlorite in cratonic peridotite xenoliths. Abundances of chlorite that potentially explain velocity reductions at MLD depths can at best be argued in locally hydrated domains at the colder and the shallower conditions where MLD occurrences have been reported.

Considering that amphibole and phlogopite can coexist at MLD depths, the effect of the absence of one phase on the variation in aggregate V_S must be evaluated keeping track of the possible abundance of the other (Fig. 6). We note that aggregate V_S decreases with increases in amphibole and phlogopite mode. For a given phlogopite abundance, with increasing amphibole mode from 0 to 10 vol.%, V_S can drop from \sim 4.6 km/s to \sim 4.5 km/s (Fig. 6a). Similarly, for a given amphibole abundance, with increasing phlogopite abundance from 0 to 5 vol.%, V_S drops from

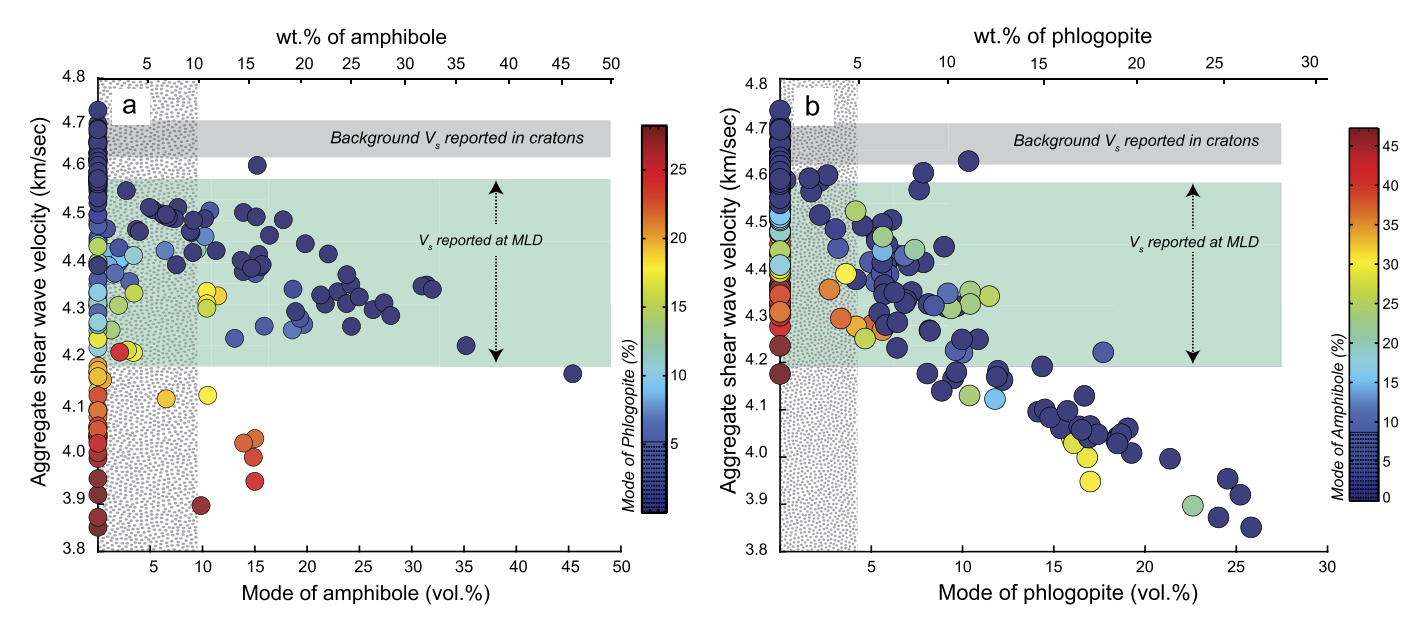


Fig. 6. Variation in estimated aggregate V_S with (a) amphibole and (b) phlogopite abundance from experimental phase relations of hydrous (\pm carbonated) peridotite systems. The symbols in panel (a) and (b) are color coded for the abundance of phlogopite and amphibole, respectively. The grey horizontal bands mark the range of V_S reported for globally-averaged Archean and early Proterozoic regions from French et al. (2013); values range from 4.62 km/s at 60 km to 4.71 km/s at 150 km, and because MLDs are intermittent and vary in depth, these global averages are likely similar to background velocity structure. The green horizontal bands represent V_S reductions reported at MLDs in cratons (Hopper and Fischer, 2018) applied to the French et al. (2013) V_S values. The bracketed amphibole (up to 10 vol.%) and phlogopite (up to 5 vol.%) abundances expected in a depleted cratonic peridotite composition are marked by the grey, vertical stippled bands. (For interpretation of the colors in the figure(s), the reader is referred to the web version of this article.)

 \sim 4.6 km/s to \sim 4.4 km/s (Fig. 6b). Thus, with the maximum abundance and compositions of amphibole, phlogopite, and magnesite that may be stable in the average cratonic SCLM, the aggregate V_S can be lowered by a maximum of 4.2-4.3%. If, however, K_2O mass balance is considered with the dominant K_2O abundance in the SCLM (Fig. 1), which leads to <2 vol.% of phlogopite, the maximum possible reduction of V_S becomes 2.01 to 3.0% depending on the choice of geotherm. Therefore, the maximum possible V_S reduction caused by volatile-bearing mineral phases can explain the lower range of velocity reductions reported at MLD depths (Fig. 6).

While the abundances of the volatile-bearing phases bracketed here can explain a fraction of the observed velocity reductions at MLD, the interplay and relative contributions of low velocity phases like pargasite and phlogopite are noteworthy. For example, for assemblages with pargasite as the only volatile-bearing phase, the aggregate V_S estimated using updated elastic constants is lower than those estimated by using the elastic moduli from the Abers and Hacker (2016) database (Fig. 7). These results are consistent with the new elastic constants for pargasite presented in this study, which suggest that pargasite is seismically slower than previously thought (Fig. 5). In contrast, for assemblages with phlogopite as the only volatile bearing phase, aggregate V_S estimates are higher when using updated elastic moduli for the different mineral end members (Table 1, Fig. 5). Assemblages where both pargasite and phlogopite are stable, the effect of pargasitic amphibole on the aggregate V_S is counterbalanced by the effect of phlogopite as evident in Fig. 7.

The range of observed velocity reductions bracketed here is estimated based on global averages of absolute values of V_S reported in Archean and early Proterozoic cratonic regions (French et al., 2013). However, background aggregate V_S depends on an interplay of factors such as temperature variations along a geotherm and abundance and composition of mineral phases stable in the cratonic SCLM. To evaluate how well the combination of these factors explains velocity reductions observed at MLD depths, we investigate V_S -depth profiles for three stations from the continental U.S. in the following section.

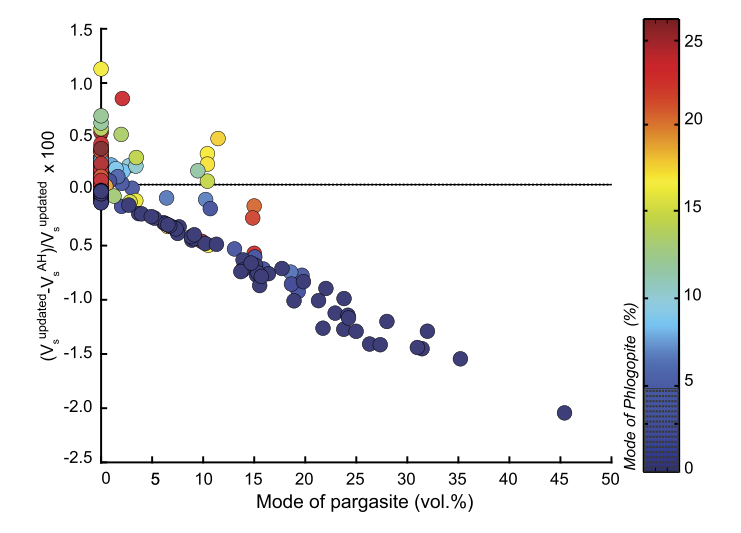


Fig. 7. Comparison of aggregate shear wave velocities estimated using updated values elastic constants for relevant end members ($V_S^{updated}$; Table 1) with those estimated using existing values from Abers and Hacker (2016) database (V_S^{AH}). The difference in estimated aggregate V_S (in percentage) is plotted as a function of pargasite abundance from experimental database. The symbols are color coded for phlogopite abundance. Positive values indicate faster V_S estimates compared to previously estimated values while negative values indicate slower V_S estimates compared to previously estimated values. With no phlogopite in the assemblage, which is expected for an extremely K-depleted SCLM, up to 10% amphibole in peridotite will lead to $\sim 0.5\%$ lower aggregate V_S than previously thought. (For interpretation of the colors in the figure(s), the reader is referred to the web version of this article.)

4.2. Volatile-bearing mineral phases across MLD depths: insights from inversion of Rayleigh waves and converted body waves in the northern continental U.S.

In order to assess the extent to which velocity reductions with depth beneath the continental U.S. can be explained by the presence of volatile-bearing mineral phases, in this section, we compare V_S -depth profiles for compositions representative of

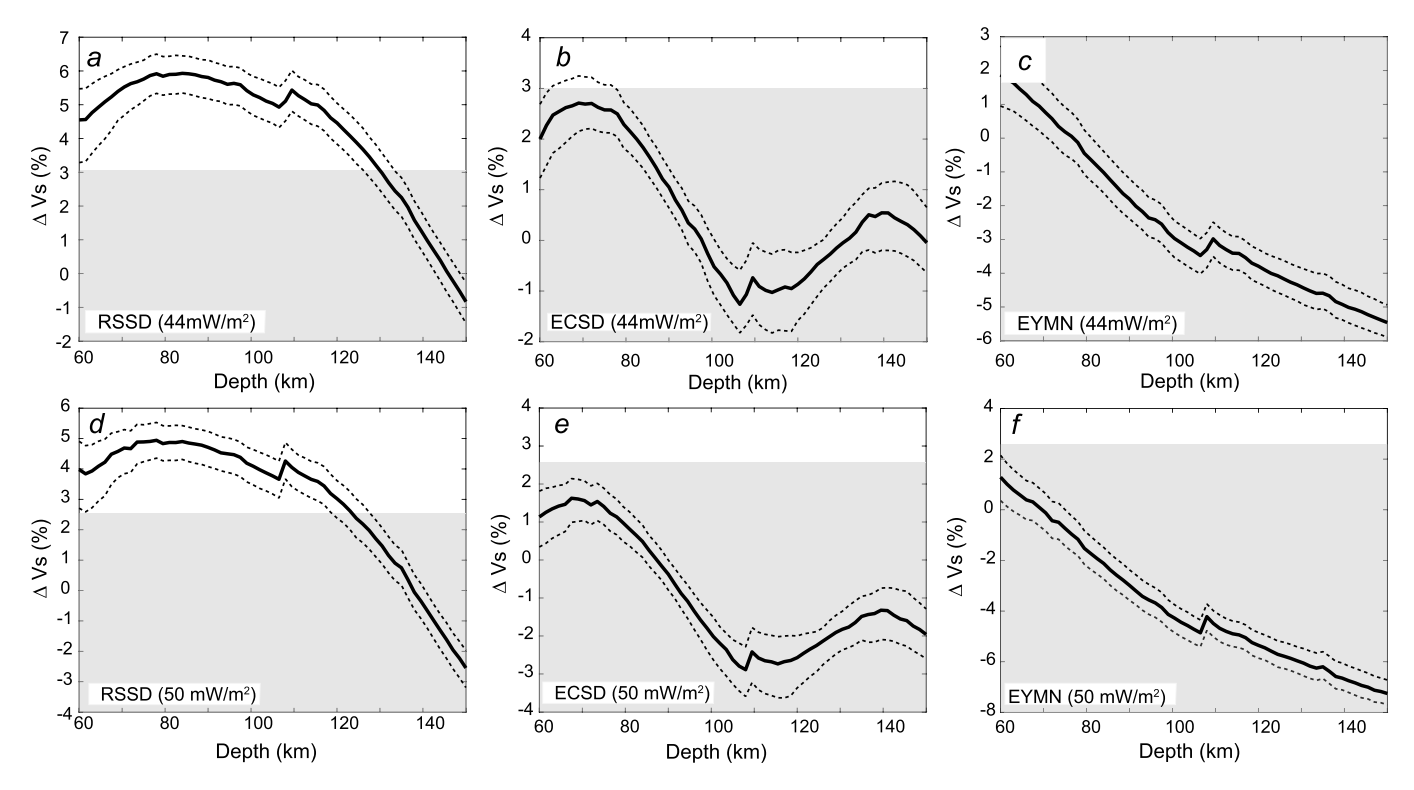


Fig. 8. Variation in $\%\Delta V_S$ as a function of depth along the 44 mW/m² (a-c) and 50 mW/m² (d-f) cratonic geotherm for representative SCLM composition DP2 for seismic stations RSSD, ECSD and EYMN (thick black lines) from Eilon et al. (2018). The thin dashed lines depict the one standard deviation uncertainties in $\%\Delta V_S$. Grey bands correspond to the range of $\%\Delta V_S$ that can be explained by the dominant mode of phlogopite (\sim 2.1 vol.%), pargasite (\sim 10 vol.%) and magnesite (\sim 0.2 vol.%) expected in the SCLM. Region above the grey band corresponds to the estimated excess $\%\Delta V_S$ for each station. Similar calculations using background SCLM composition DP1 is presented in Fig. S6.

metasomatized cratonic SCLM domains to V_S-depth profiles obtained by the inversion of Rayleigh wave phase velocities and Ps and Sp body wave stacks for three seismic stations in cratonic regions of the northern U.S. (Eilon et al., 2018). Here we define $\%\Delta V_S$ as the percent deviation of the measured V_S for each station from Eilon et al. (2018) (V_S station) from the expected background shear wave velocity profile for unmetasomatized depleted peridotite mantles (V_{SB}). In other words, $\%\Delta V_S = 100 \times$ $(V_{SB}\text{-}V_S^{\,station})/V_{SB}$. Variation in $\%\Delta V_S$ with depth for each station was determined with background V_S values (V_{SB}) along two representative cratonic geotherms (~44 and 50 mW/m² surface heat flux; Fig. 8). V_{SB} along the geotherms was estimated using the stable equilibrium mineral assemblages for two unmetasomatized peridotite compositions: (1) the dominant peridotite composition in the cratonic SCLM, based on the most abundant oxide distributions in cratonic peridotite xenoliths (DP2 in Fig. 1 (c-h); Fig. 8) and (2) a model depleted peridotite composition (e.g., Saha et al., 2018; DP1 - Fig. S6). In both cases, the equilibrium mineral assemblages (in vol.%) as a function of depth were obtained using Perple_X (Connolly, 2005). For this calculation, the database of Stixrude and Lithgow-Bertelloni (2011) for mineral properties and solution models was chosen to allow inclusion of different end members of the minerals expected in the mantle rocks. The mineral proportions estimated are reported in Tables S9 and S10.

Aggregate V_S for the unmetasomatized compositions (V_{SB}) was estimated using the updated Abers and Hacker (2016) database and estimates of modal abundance (vol.%) and phase compositions for the mineral end members. $\&\Delta V_S$ for individual seismic stations was then calculated for the MLD depth range i.e., 60 km to \sim 150 km (reported in Tables S9 and S10) both for background mantle composition DP2 (Fig. 8) and DP1 (Fig. S6).

The magnitude of $\%\Delta V_S$ for each station varies primarily as a function of the choice of the cratonic geotherm and also to

some extent as a function of the background wave speed of the unmetasomatized peridotite (Fig. 8 and S6). Comparison between Fig. 8 and Fig. S6 reveals that the influence of cratonic geotherm variation for equivalent surface heat flux of 50 to 44 mW/m² is larger than the subtle variation in the ambient mantle composition. We note that the maximum range of estimated velocity reductions varies across the three seismic stations. For station RSSD, the maximum range of $\%\Delta V_S$ is $\sim\!5.8$ to 6.0% along the 44 mW/m² geotherm and $\sim\!4.6$ to 4.9% along the 50 mW/m² geotherm. For station ECSD the maximum range of ΔV_S varies from 2.6 to 2.7% along the 44 mW/m² geotherm and from 1.6 to 1.9% along the 50 mW/m². For station EYMN, the maximum range of $\%\Delta V_S$ varies from 1.5 to 1.7% along the 44 mW/m² geotherm and from 1.0 to 1.3% along the 50 mW/m² geotherm.

The maximum abundances of phlogopite (\sim 2 vol.%; bulk H₂O of \sim 800 ppm), pargasite (\sim 10 vol.%; bulk H₂O of \sim 2000 ppm) and magnesite (\leq 0.2 vol.%; bulk CO₂ \leq \sim 1000 ppm) that can be stabilized in the dominant (most depleted) cratonic SCLM bulk can explain ΔV_S up to 2.6-3.0% along the 44 mW/m² geotherm and 2.6-2.8% along the 50 mW/m² geotherm (marked as grey bands in Fig. 8 and Fig. S6). While this bracketed reduction can mostly explain the velocity reductions estimated for stations ECSD and EYMN, this is only a fraction of % ΔV_S estimated for station RSSD.

To eliminate these differences in $\%\Delta V_S$ for RSSD, we further estimate the volatile-bearing mineral abundances required to explain the full range of excess $\%\Delta V_S$ by relaxing the reference bulk composition from being fixed at the most depleted SCLM composition (Fig. 1). Given the uncertainty in the CO_2 abundance of SCLM and the low likelihood that the magnesite mode exceeds 1 vol.%, we primarily consider amphibole and phlogopite for this comparison. The excess $\%\Delta V_S$ for station RSSD varies from 0-3.2% along the 44 mW/m² and 0-2.0% along the 50 mW/m² geotherm using DP1 as the background, and 0-3.0% along the 44 mW/m² and 0-2.1%

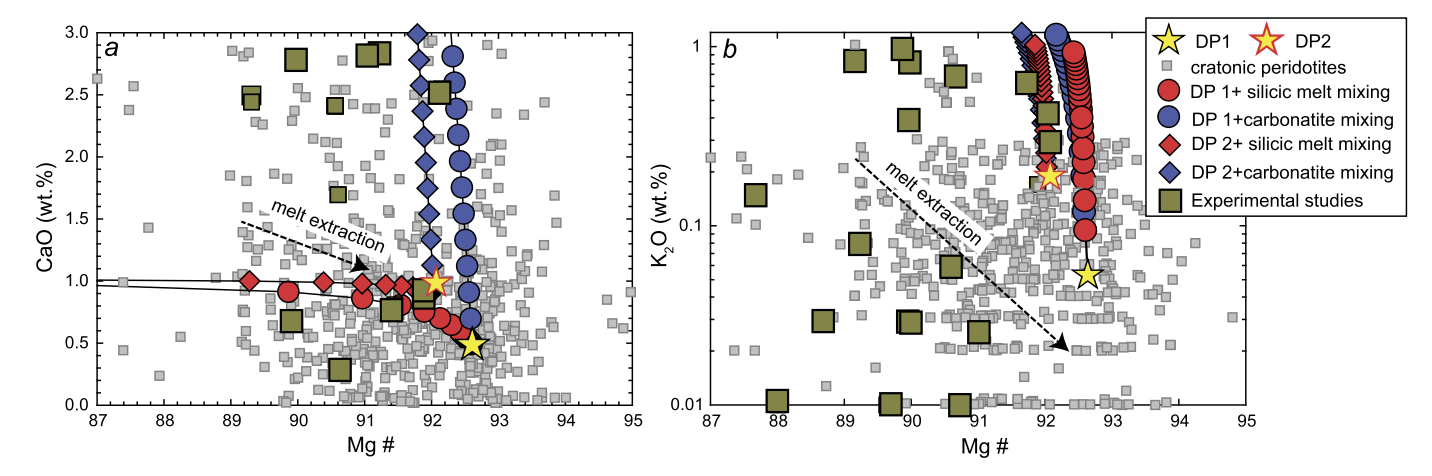


Fig. 9. Variation in (a) CaO and (b) K₂O contents (in wt%) as a function of Mg# when a hydrous silicic melt (red symbols) or a carbonatitic melt (blue symbols) of variable proportion infiltrates DP1 and DP2 depleted peridotite (shown in Fig. 1). Plotted for comparison are SCLM peridotite compositions. Each circle or diamond represents a 1% increment of two example melt component additions that can potentially metasomatize the depleted peridotite during craton formation. The melt components used for the mixing calculations are given in Table S8. Also plotted for comparison are experimental compositions that can conceivably result from compositional heterogeneity imparted by one of these processes or the original fertility level set by a melt extraction event(s) and can result in sufficient abundance of hydrous silicate phases to explain MLDs.

along the 50 mW/m² geotherm using DP2 as the background. In order to erase these differences, additional amounts of phlogopite (\sim 8.0-10.0 vol.%) or pargasitic amphibole (\sim 15.6-17.0 vol.%) would be required.

The abundances of volatile-bearing phases required to explain the maximum range of velocity reductions estimated at MLD depths for the seismic station RSSD in the northern continental U.S. are distinctly higher than those that are expected in a dominantly depleted cratonic SCLM bulk composition. Figs. 3, 4, and 6 suggest that in order to satisfy the full range of excess velocity reductions observed at RSSD, as much as $\sim\!25$ vol.% amphibole ($\sim\!5000$ ppm H_2O) or $\sim\!15$ vol.% phlogopite ($\sim\!6000$ ppm H_2O) is required. Hence we suggest that modal metasomatism caused by volatile influx can only account for a small fraction of the total velocity reduction estimated for this station.

If the entire non-volatile, major and minor element compositional range of SCLM xenoliths is considered, the lower range of velocity reductions reported at MLD depths can be explained (also discussed in section 4.1). However, such widespread metasomatism globally is not expected, especially because the necessary compositional fertility would not only require major and minor element compositions of SCLM beyond the dominant mode sampled by xenoliths but also require too extreme bulk H₂O and/or CO₂ contents.

4.3. Nature of SCLM metasomatism and craton formation – insights from MLDs

Although we argue that only a small fraction of the maximum observed V_S reduction can be achieved by the presence of volatile-bearing mineral phases, another key question is whether the presence of such hydrous or carbonate phases require recent fluid addition. Our assessment of phase equilibria, with updated elasticity constraints for the volatile-bearing phases, sheds light on the feasibility of formation of metasomatic domains in the cratonic SCLM. The main trend of cratonic SCLM compositions relates to variable extent of basaltic melt depletion and/or refertilization (Fig. 9). However, the width of the trend can be influenced by other metasomatic processes in addition to being the residue of a polybaric near fractional melting process (e.g. Walter, 1998, 1999). It is evident from Fig. 9 that the addition of hydrous ($\pm CO_2$) silicic melt (derived from subducting slabs; e.g., Duncan and Dasgupta, 2014; Muth et al., 2020), or hydrous carbonatitic melt or other CO2-rich melts from subducting slabs or the ambient or plume

mantle (e.g., Poli, 2015; Dasgupta, 2018; Sun and Dasgupta, 2020) to an ultra-depleted peridotite, during craton formation may add to the compositional heterogeneity of cratonic SCLM. However, based on the overlap between the experimental peridotite and natural cratonic peridotite bulk compositions (Fig. 1), metasomatism cannot introduce the high abundances of phlogopite and amphibole required to explain the entire range of MLD-associated velocity reductions observed at MLD. The metasomatic alterations, however, can be expected during various modes of craton formation such as accretion and thickening of sub-arc mantle and imbrication of subducting slabs, stabilizing amphibole and phlogopite abundances that can explain lower velocity reductions observed at MLD depths even if only the dominant major and minor elemental composition of SCLM is considered.

5. Concluding remarks

We test whether reductions in aggregate V_S at mid-lithospheric depths in cratons can be explained by the presence of hydrous and carbonate mineral phases. By compiling the existing high pressure-temperature experiments in peridotite + H_2O , peridotite + CO_2 , and peridotite + CO_2 systems and finding the compositional overlap with natural cratonic SCLM xenolith database, we constrain the nature, compositions, and proportions of volatile-bearing mineral phases expected in the average, global cratonic mantle.

We find that for the whole depth range over which MLDs have been imaged seismically, chlorite, pargasitic amphibole, phlogopite, and magnesite are possible stable phases. However, given the thermal structure of cratons and the upper limit on bulk CO2 content, pargasitic amphibole and phlogopite are the most likely globally relevant phases that can explain MLDs. To accurately determine the aggregate V_S, we calculate elastic constants for pargasite and their pressure and temperature derivatives and update the thermoelastic databases for other relevant mineral end members. Specifically, we determine that pargasite is seismically slower by 4%-8% than previously thought. Based on the dominant CaO and K2O contents of cratonic peridotite xenoliths and estimated upper limits on the CO_2 content of cratonic SCLM, we show that $\leq \sim 10$ vol.% amphibole, <~2 vol.% phlogopite and ≤~0.2 vol.% magnesite solid solution can be expected in the cratonic SCLM. For a fixed cratonic SCLM bulk composition, the combination of amphibole, phlogopite and magnesite bracketed here can explain a maximum of 2.0-3.0% reduction in aggregate V_S corresponding to the lower-

range of velocity reductions reported at MLDs. However, this is the maximum velocity reduction that can be achieved using the highest possible abundance of phlogopite, pargasitic amphibole, and magnesite solid solution in dominant major and minor elemental, non-volatile compositional range of SCLM. Given that the combined presence of 2% phlogopite and 10% pargasite would require as much as ~ 3000 ppm H₂O in SCLM, this upper limit is considered a strict upper limit because of the dehydrated nature of SCLM (e.g., Peslier et al., 2010). Comparison of our estimated velocities of metasomatized assemblages with the V_S-depth profiles for three specific stations in the continental U.S., using model background compositions, reveals that the abundances of amphibole, phlogopite and magnesite bracketed here can explain 2.01 to 3.01% reduction in aggregate V_S depending on the choice of background wave velocities of unmetasomatized peridotite and the geotherm. The excess abundances of amphibole (~25 vol.%) and phlogopite (~15 vol.%) that are needed to explain the entire range of measured velocity reductions cannot be supported by the dominant major element compositional range of SCLM. Therefore, a key conclusion arising from our study is that, in contradiction to the claims in many recent studies (e.g., Rader et al., 2015; Hopper and Fischer, 2015; Eeken et al., 2018; Saha et al., 2018), the largest velocity reduction at MLD depths in cratons cannot be explained by the presence of volatile-bearing mineral phases. In other words, unless regions with high-end MLD velocity reductions represent highly anomalous mantle compositions not represented by cratonic peridotite xenoliths and the estimated upper limit of CO₂ and H₂O contents in SCLM, alternate mechanisms for velocity reductions, including elastically accommodated grain boundary sliding (Karato et al., 2015; Karato and Park, 2018), must be considered even if volatile-induced modal metasomatism is part of the cause. Yet, a fraction of the estimated V_S reduction can indeed be caused by phases such as pargasite, and formation of pargasite and/or phlogopite at MLD depths does not require the volatile-induced metasomatism to be recent. The major element compositional spectrum of SCLM xenoliths does allow volatile metasomatism aided by fluid and/or hydrous or carbonated melt infiltration. Such interaction at MLD depths is consistent with at least two models of craton formation associated with subduction zones.

CRediT authorship contribution statement

Sriparna Saha: Data curation, Formal analysis, Investigation, Methodology, Validation, Visualization, Writing - original draft, Writing - review & editing. **Ye Peng:** Data curation, Formal analysis, Investigation, Methodology, Software, Validation, Visualization, Writing - original draft, Writing - review & editing. **Rajdeep Dasgupta:** Conceptualization, Data curation, Funding acquisition, Methodology, Project administration, Resources, Supervision, Writing - review & editing. **Mainak Mookherjee:** Data curation, Funding acquisition, Methodology, Project administration, Resources, Supervision, Writing - review & editing. **Karen M. Fischer:** Conceptualization, Data curation, Funding acquisition, Methodology, Project administration, Resources, Supervision, Writing - review & editing.

Declaration of competing interest

The authors declare that they have no known competing financial interests or personal relationships that could have appeared to influence the work reported in this paper.

Acknowledgements

We acknowledge two anonymous reviewers for their useful reviews. We also thank Shun Karato and an anonymous reviewer for

providing critical review on an earlier version of this paper. The research was supported by NSF CSEDI grants EAR-1763226 (R.D.), EAR-1763215 (M.M.), and EAR-1763243 (K.M.F.). R.D. also acknowledges research support from NSF grant EAR-1255391. M.M. also acknowledges research support from NSF grant EAR-1753125 and XSEDE resources (TG-GE0170003).

Appendix A. Supplementary material

Supplementary material related to this article can be found online at https://doi.org/10.1016/j.epsl.2020.116602.

References

- Abers, G., Hacker, B.R., 2016. A MATLAB toolbox and Excel workbook for calculating the densities, seismic wave speeds, and major element composition of minerals and rocks at pressure and temperature. Geochem. Geophys. Geosyst., 1–21. https://doi.org/10.1002/2015GC006171.
- Abt, D.L., Fischer, K.M., French, S.W., Ford, H.A., Yuan, H., Romanowicz, B., 2010. North American lithospheric discontinuity structure imaged by Ps and Sp receiver functions. J. Geophys. Res. 115, 1–24. https://doi.org/10.1029/ 2009JB006914.
- Artemieva, I.M., 2009. The continental lithosphere: reconciling thermal, seismic, and petrologic data. Lithos 109, 23–46. https://doi.org/10.1016/j.lithos.2008.09.015.
- Bezacier, L., Reynard, B., Bass, J.D., Wang, J., Mainprice, D., 2010. Elasticity of glaucophane, seismic velocities and anisotropy of the subducted oceanic crust. Tectonophysics 494, 201–210. https://doi.org/10.1016/j.tecto.2010.09.011.
- Boyd, F.R., 1989. Compositional distinction between oceanic and cratonic lithosphere. Earth Planet. Sci. Lett. 96, 15–26. https://doi.org/10.1016/0012-821X(89) 90120-9
- Brown, J.M., Abramson, E.H., 2016. Elasticity of calcium and calcium-sodium amphiboles. Phys. Earth Planet. Inter. 261, 161–171. https://doi.org/10.1016/j.pepi. 2016.10.010.
- Canil, D., 1990. Experimental study bearing on the absence of carbonate in mantlederived xenoliths. Geology 18, 1011–1013.
- Chheda, T.D., Mookherjee, M., Mainprice, D., Dos Santos, A.M., Molaison, J.J., Chantel, J., Manthilake, G., Bassett, W.A., 2014. Structure and elasticity of phlogopite under compression: geophysical implications. Phys. Earth Planet. Inter. 233, 1–12. https://doi.org/10.1016/j.pepi.2014.05.004.
- Comodi, P., Mellini, M., Ungaretti, L., Zanazzi, P.F., 1991. Compressibility and high pressure structure refinement of tremolite, pargasite and glaucophane. Eur. J. Mineral. 3, 485–500. https://doi.org/10.1127/ejm/3/3/0485.
- Connolly, J.A.D., 2005. Computation of phase equilibria by linear programming: a tool for geodynamic modeling and its application to subduction zone decarbonation. Earth Planet. Sci. Lett. 236, 524–541. https://doi.org/10.1016/j.epsl.2005.
- Cooper, C.M., Miller, M.S., 2014. Craton formation: internal structure inherited from closing of the early oceans. Lithosphere 6, 35–42. https://doi.org/10.1130/L321.1.
- Dasgupta, R., Hirschmann, M.M., 2006. Melting in the Earth's deep upper mantle caused by carbon dioxide. Nature 440, 659–662. https://doi.org/10.1038/nature04612.
- Dasgupta, R., 2018. Volatile bearing partial melts beneath oceans and continents where, how much, and of what compositions? Am. J. Sci. 318, 141–165.
- Duncan, M.S., Dasgupta, R., 2014. CO₂ solubility and speciation in rhyolitic, sediment partial melts at 1.5-3.0 GPa implications for carbon flux in subduction zones. Geochim. Cosmochim. Acta 124, 328–347.
- Dvir, O., Pettke, T., Fumagalli, P., Kessel, R., 2011. Fluids in the peridotite-water system up to 6 GPa and 800 °C: new experimental constrains on dehydration reactions. Contrib. Mineral. Petrol. 161, 829–844. https://doi.org/10.1007/s00410-010-0567-2.
- Eeken, T., Goes, S., Pedersen, H.A., Arndt, N.T., Bouilhol, P., 2018. Seismic evidence for depth-dependent metasomatism in cratons. Earth Planet. Sci. Lett. 491, 148–159. https://doi.org/10.1016/j.epsl.2018.03.018.
- Eilon, Z., Fischer, K.M., Dalton, C.A., 2018. An adaptive Bayesian inversion for upper mantle structure using surface waves and scattered body waves Bayesian joint inversion. Geophys. J. Int. 214, 232–253. https://doi.org/10.1093/gji/ggy137.
- Falloon, T.J., Green, D.H., 1989. The solidus of carbonated, fertile peridotite. Earth Planet. Sci. Lett. 94, 364–370. https://doi.org/10.1016/0012-821X(89)90153-2.
- Fischer, K.M., Ford, H.A., Abt, D.L., Rychert, C.A., 2010. The lithosphere-asthenosphere boundary. Annu. Rev. Earth Planet. Sci. 38, 551–575. https://doi.org/10.1146/annurev-earth-040809-152438.
- Foley, S.F., Fischer, T., 2017. An essential role for continental rifts and lithosphere in the deep carbon cycle. Nat. Geosci. 10, 897–902.
- Ford, H., Long, M.D., Wirth, E.A., 2016. Midlithospheric discontinuities and complex anisotropic layering in the mantle lithosphere beneath the Wyoming and Superior Provinces. J. Geophys. Res., Solid Earth 121, 6675–6697. https://doi.org/10.1002/2016/B012978.

- French, S., Lekic, V., Romanowicz, B., 2013. Waveform tomography reveals channeled flow at the base of the oceanic asthenosphere. Science 342, 227–230. https://doi.org/10.1126/science.1241514.
- Fumagalli, P., Poli, S., 2005. Experimentally determined phase relations in hydrous peridotites to 6.5 GPa and their consequences on the dynamics of subduction zones. J. Petrol. 46, 555–578. https://doi.org/10.1093/petrology/egh088.
- Green, D.H., Hibberson, W.O., Rosenthal, A., Kovacs, I., Yaxley, G.M., Falloon, T.J., Brink, F., 2014. Experimental study of the influence of water on melting and phase assemblages in the upper mantle. J. Petrol. 55, 2067–2096. https://doi.org/10.1093/petrology/egu050.
- Griffin, W.L., O'Reilly, S.Y., S, A., 1988. Mantle metasomatism beneath western Victoria, Australia: II. isotopic geochemistry of Cr-diopside lherzolites and Al-augite pyroxenites. Geochim. Cosmochim. Acta 52, 449–459. https://doi.org/10.1016/0016-7037(88)90100-7.
- Grove, T., Chatterjee, N., Parman, S., Medard, E., 2006. The influence of H₂O on mantle wedge melting. Earth Planet. Sci. Lett. 249, 74–89. https://doi.org/10.1016/j.epsl.2006.06.043.
- Gung, Y., Panning, M., Romanowicz, B., 2003. Global anisotropy and the thickness of continents. Nature 422, 707–711. https://doi.org/10.1038/nature01559.
- Hansen, S.M., Dueker, K., Schmandt, B., 2015. Thermal classification of lithospheric discontinuities beneath USArray. Earth Planet. Sci. Lett. 431, 36–47. https://doi. org/10.1016/j.epsl.2015.09.009.
- Hohenberg, P., Kohn, W., 1964. Inhomogenous electron gas. Phys. Rev. 40, 391–402. https://doi.org/10.1007/BF01198136.
- Holland, T.J.B., Powell, R., 1998. An internally consistent thermodynamic data set for phases of petrological interest. J. Metamorph. Geol. 16, 309–343. https://doi.org/10.1111/j.1525-1314.1998.00140.x.
- Hopp, J., Trieloff, M., Brey, G.P., Woodland, A.B., Simon, N.S.C., Wijbrans, J.R., Siebel, W., Reitter, E., 2008. 40 Ar/³⁹ Ar-ages of phlogopite in mantle xenoliths from South African kimberlites: evidence for metasomatic mantle impregnation during the Kibaran orogenic cycle. Lithos 106, 351–364. https://doi.org/10.1016/j.lithos.2008.09.001.
- Hopper, E., Fischer, K.M., 2018. The changing face of the lithosphere-asthenosphere boundary: imaging continental scale patterns in upper mantle structure across the contiguous U.S. with sp converted waves. Geochem. Geophys. Geosyst. 19, 2593–2614. https://doi.org/10.1029/2018GC007476.
- Hopper, E., Fischer, K.M., 2015. The meaning of midlithospheric discontinuities: a case study in the northern U.S. craton. Geochem. Geophys. Geosyst. 18, 1541–1576. https://doi.org/10.1002/2014GC005684.
- Jordan, T.H., 1978. Composition and development of the continental tectosphere. Nature 274, 544–548. https://doi.org/10.1038/274544a0.
- Karato, S., Olugboji, T., Park, J., 2015. Mechanisms and geologic significance of the mid-lithosphere discontinuity in the continents. Nat. Geosci. 8, 509–514. https:// doi.org/10.1038/ngeo2462.
- Karato, S., Park, J., 2018. On the origin of the upper mantle seismic discontinuities.In: Lithospheric Discontinuities. In: Geophys. Monograph Series.
- Kind, R., Yuan, X., 2018. Perspectives of the S-receiver-function method to image upper mantle discontinuities. Lithospheric Discontinuities, Geophys. Monograph Series. https://doi.org/10.1002/9781119249740.ch8.
- Lara, M., Dasgupta, R., 2020. Partial melting of a depleted peridotite metasomatized by a MORB-derived hydrous silicate melt - implications for subduction zone magmatism. Geochim. Cosmochim. Acta 290, 137–161. https://doi.org/10.1016/j. gca.2020.09.001.
- Lee, C.-T.A., Jiang, H., Dasgupta, R., Torres, M., 2019. A framework for understanding whole-Earth carbon cycling. In: Orcutt, B., Daniel, I., Dasgupta, R. (Eds.), Deep Carbon: Past to Present. Cambridge University Press, pp. 313–357.
- Lee, C.-T.a., Luffi, P., Chin, E.J., 2011. Building and destroying continental mantle. Annu. Rev. Earth Planet. Sci. 39, 59–90. https://doi.org/10.1146/annurev-earth-040610-133505.
- Luguet, A., Behrens, M., Pearson, D.G., Konig, S., Herwartz, D., 2015. Significance of the whole rock Re–Os ages in cryptically and modally metasomatised cratonic peridotites: constraints from HSE–Se–Te systematics. Geochim. Cosmochim. Acta 164, 441–463. https://doi.org/10.1016/j.gca.2015.06.016.
- Mallik, A., Nelson, J., Dasgupta, R., 2015. Partial melting of fertile peridotite fluxed by hydrous rhyolitic melt at 2–3 GPa: implications for mantle wedge hybridization by sediment melt and generation of ultrapotassic magmas in convergent margins. Contrib. Mineral. Petrol. https://doi.org/10.1007/s00410-015-1139-2.
- Mandler, B.E., Grove, T.L., 2016. Controls on the stability and composition of amphibole in the Earth's mantle. Contrib. Mineral. Petrol. 171, 68. https://doi.org/10.1007/s00410-016-1281-5.
- Mengel, K., Green, D.H., 1989. Stability of amphibole and phlogopite in metasomatized peridotite under water-saturated and water-undersaturated conditions. In: Kimberlites Relat. Rocks, vol. 1, pp. 571–581.
- Mookherjee, M., Bezacier, L., 2012. The low velocity layer in subduction zone: structure and elasticity of glaucophane at high pressures. Phys. Earth Planet. Inter. 208, 50–58. https://doi.org/10.1016/j.pepi.2012.07.007.
- Mookherjee, M., Mainprice, D., 2014. Unusually large shear wave anisotropy for chlorite in subduction zone settings. Geophys. Res. Lett. 41, 1506–1513. https:// doi.org/10.1002/2014GL059334.

- Muth, M., Duncan, M.S., Dasgupta, R., 2020. The effect of variable Na/K on CO₂ solubility in slab-derived rhyolitic melts. In: Manning, C., Lin, A., Mao, W. (Eds.), Carbon in Earth's Interior. In: Geophysical Monograph, vol. 249, pp. 195–208.
- Peng, Y., Mookherjee, M., 2020. Thermoelasticity of tremolite amphibole: geophysical implications. Am. Mineral. 105, 904–916. https://doi.org/10.2138/am-2020-7189
- Peslier, A.H., Woodland, A.B., Bell, D.R., Lazarov, M., 2010. Olivine water contents in the continental lithosphere and the longevity of cratons. Nature 467, 78–81. https://doi.org/10.1038/nature09317.
- Poli, S., 2015. Carbon mobilized at shallow depths in subduction zones by carbonatitic liquids. Nat. Geosci. 8, 633–636.
- Rader, E., Emry, E., Schmerr, N., Frost, D., Cheng, C., Menard, J., Yu, C., Geist, D., 2015. Characterization and petrological constraints of the mid-lithospheric discontinuity. Geochem. Geophys. Geosyst. 16, 3484–3504.
- Rychert, C.A., Shearer, P.M., 2009. A global view of the lithosphere-asthenosphere boundary. Science 324, 444–448. https://doi.org/10.1126/science.1169754.
- Saha, S., Dasgupta, R., 2019. Phase relations of a depleted peridotite fluxed by a CO₂-H₂O fluid implications for the stability of partial melts versus volatile-bearing mineral phases in the cratonic mantle. J. Geophys. Res., Solid Earth 124, 10089–10106. https://doi.org/10.1029/2019JB017653.
- Saha, S., Dasgupta, R., Tsuno, K., 2018. High pressure phase relations of a depleted peridotite fluxed by CO₂-H₂O-bearing siliceous melts and the origin of midlithospheric discontinuity. Geochem. Geophys. Geosyst. 19, 595–620. https://doi.org/10.1002/2017GC007233.
- Selway, K., 2019. Electrical discontinuities in the continental lithosphere imaged with magnetotellurics. Lithospheric Discontinuities, Geophys. Monograph Series. https://doi.org/10.1002/9781119249740.ch5.
- Selway, K., Ford, H., Kelemen, P., 2015. The seismic mid-lithosphere discontinuity. Earth Planet. Sci. Lett. 414, 45–57. https://doi.org/10.1016/j.epsl.2014.12.029.
- Sieber, M.J., Hermann, J., Yaxley, G.M., 2018. An experimental investigation of C-O-H fluid-driven carbonation of serpentinites under forearc conditions. Earth Planet. Sci. Lett. 496, 178–188. https://doi.org/10.1016/j.epsl.2018.05.027.
- Shearer, P.M., Buehler, J., 2019. Imaging upper-mantle structure under USArray using long-period reflection seismology. J. Geophys. Res., Solid Earth 124, 9638–9652. https://doi.org/10.1029/2019JB017326.
- Steinberger, B., Becker, T.W., 2018. A comparison of lithospheric thickness models. Tectonophysics 746, 325–338. https://doi.org/10.1016/j.tecto.2016.08.001.
- Stixrude, L., Lithgow-Bertelloni, C., 2011. Thermodynamics of mantle minerals II.

 Phase equilibria. Geophys. J. Int. 184, 1180–1213. https://doi.org/10.1111/j.1365-246X 2010.04890 x
- Sun, C., Dasgupta, R., 2019. Slab-mantle interaction, carbon transport, and kimber-lite generation in the deep upper mantle. Earth Planet. Sci. Lett. 506, 38–52. https://doi.org/10.1016/j.epsl.2018.10.028.
- Sun, C., Dasgupta, R., 2020. Thermobarometry of CO₂-rich, silica-undersaturated melts constrains cratonic lithosphere thinning through time in areas of kimberlitic magmatism. Earth Planet. Sci. Lett. 550, 116549. https://doi.org/10.1016/ j.epsl.2020.116549.
- Thybo, H., 2006. The heterogeneous upper mantle low velocity zone. Tectonophysics 416, 53–79. https://doi.org/10.1016/j.tecto.2005.11.021.
- Till, C.B., Grove, T.L., Withers, A.C., 2012. The beginnings of hydrous mantle wedge melting. Contrib. Mineral. Petrol. 163, 669–688. https://doi.org/10.1007/s00410-011-0692-6.
- Tommasi, A., Langone, A., Padrón-Navarta, J.A., Zanetti, A., Vauchez, A., 2017. Hydrous melts weaken the mantle, crystallization of pargasite and phlogopite does not: insights from a petrostructural study of the Finero peridotites, southern Alps. Earth Planet. Sci. Lett. 477, 59–72. https://doi.org/10.1016/j.epsl.2017.08. 015.
- Tumiati, S., Fumagalli, P., Tiraboschi, C., Poli, S., 2013. An experimental study on COH-bearing peridotite up to 3.2 GPa and implications for crust-mantle recycling. J. Petrol. 54, 453–479. https://doi.org/10.1093/petrology/egs074.
- Walter, M.J., 1998. Melting of garnet peridotite and the origin of komatiite and depleted lithosphere. J. Petrol. 39, 29–60.
- Walter, M.J., 1999. Melting residues of fertile peridotite and the origin of cratonic lithosphere. In: Fei, Y., Bertka, C.M., Mysen, B.O. (Eds.), Mantle Petrology: Field Observations and High Pressure Experimentation: A Tribute to Francis R. (Joe) Boyd. The Geochem. Soc. Spl. Pub, vol. 6. pp. 225–239.
- Wang, Z., Kusky, T.M., 2019. The importance of a weak mid-lithospheric layer on the evolution of the cratonic lithosphere Earth-science reviews the importance of a weak mid-lithospheric layer on the evolution of the cratonic lithosphere. Earth-Sci. Rev. 190, 557-569. https://doi.org/10.1016/j.earscirev.2019.02.010.
- Wirth, E.A., Long, M.D., 2014. A contrast in anisotropy across mid-lithospheric discontinuities beneath the central United States-a relic of craton formation. Geology 42, 851–854. https://doi.org/10.1130/G35804.1.
- Wolbern, I., Rumpker, G., Link, K., Sodoudi, F., 2012. Melt infiltration of the lower lithosphere beneath the Tanzania craton and the Albertine rift inferred from S receiver functions. Geochem. Geophys. Geosyst. 13, 1–20. https://doi.org/10. 1029/2012GC004167
- Yuan, H., Romanowicz, B., 2010. Lithospheric layering in the North American craton. Nature 466, 1063–1068. https://doi.org/10.1038/nature09332.